Coding of envelopes by correlated but not single-neuron activity requires neural variability

Michael G. Metzen[a,1], Mohsen Jamali[a,1], Jérome Carriot[a], Oscar Ávila-Ákerberg[b], Kathleen E. Cullen[a], and Maurice J. Chacron[a,b,2]

[a]Department of Physiology, McGill University, Montréal, Québec, Canada H3G1Y6; and [b]Department of Physics, McGill University, Montréal, Québec, Canada H3A2T8

Edited by Charles F. Stevens, The Salk Institute for Biological Studies, La Jolla, CA, and approved March 5, 2015 (received for review October 3, 2014)

Understanding how the brain processes sensory information is often complicated by the fact that neurons exhibit trial-to-trial variability in their responses to stimuli. Indeed, the role of variability in sensory coding is still highly debated. Here, we examined how variability influences neural responses to naturalistic stimuli consisting of a fast time-varying waveform (i.e., carrier or first order) whose amplitude (i.e., envelope or second order) varies more slowly. Recordings were made from fish electrosensory and monkey vestibular sensory neurons. In both systems, we show that correlated but not single-neuron activity can provide detailed information about second-order stimulus features. Using a simple mathematical model, we made the strong prediction that such correlation-based coding of envelopes requires neural variability. Strikingly, the performance of correlated activity at predicting the envelope was similarly optimally tuned to a nonzero level of variability in both systems, thereby confirming this prediction. Finally, we show that second-order sensory information can only be decoded if one takes into account joint statistics when combining neural activities. Our results thus show that correlated but not single-neural activity can transmit information about the envelope, that such transmission requires neural variability, and that this information can be decoded. We suggest that envelope coding by correlated activity is a general feature of sensory processing that will be found across species and systems.

correlation | envelope | electrosensory | vestibular | neural coding

Although correlated activity and neural variability are both observed ubiquitously in the brain, their functional roles have been the focus of much debate (1, 2). Indeed, the conventional wisdom that both are detrimental to coding by introducing redundancy and noise, respectively, has been recently challenged (3, 4). Here, we investigated the effects of variability on the coding by correlated activity of naturalistic sensory stimuli that often have rich spatiotemporal structure characterized by first- and second-order attributes. Specifically, we considered how neural populations within the electrosensory system of weakly electric fish and the vestibular system of monkeys respond to stimuli consisting of a fast time-varying carrier waveform (i.e., first-order attribute) whose amplitude or envelope (i.e., second-order attribute) varies independently on a longer timescale. Envelopes are critical for perception (5, 6), yet their neural encoding continues to pose a challenge to investigators because they are nonlinearly related to the stimulus waveform (7). Previous studies have shown that single neurons can transmit envelope information through changes in firing rate (8, 9) when the relationship between the stimulus input and the output firing rate is nonlinear. In contrast, here, we focused on neuronal responses that were linearly related to the stimulus waveform.

Weakly electric fish generate an electric field around their body through the electric organ discharge (EOD) (for review, see ref. 10). Peripheral electroreceptor afferents scattered over the animal's skin respond to the low-intensity changes in EOD amplitude frequently encountered under natural conditions (11) through linearly related changes in firing rate (12). Although previous studies have shown that envelope information under these conditions reaches higher brain regions, thus giving rise to perception and behavior (13), the processing of low-intensity envelopes by the afferent population is not well understood.

The vestibular system provides information about head motion relative to space that is necessary for maintaining posture, computing spatial orientation, and perceiving self-motion (14). This essential system is well characterized anatomically and displays important differences with the electrosensory system. Peripheral afferents respond to head velocity through changes in firing rate that are linearly related to the stimulus (15, 16) but exhibit a much wider range of resting discharge variability than electroreceptor afferents (12). Although low-intensity envelopes are a prominent feature of vestibular signals encountered during natural self-motion (17), the neural mechanisms underlying their processing by vestibular neurons are not well understood.

Here, we show that correlated but not single-neuron activity encodes envelopes in both the electrosensory and vestibular systems. Through a combination of mathematical modeling and computational analyses, we further show that such coding is found for wide ranges of parameter values and is optimal for a nonzero level of neural variability. We suggest that correlation coding provides a general neural strategy to encode the commonly observed second-order features of sensory input across sensory systems.

Results

Correlations Between Spike Trains Encode Second-Order Stimulus Attributes. We studied neural responses to stimuli consisting of a noisy waveform (Fig. 1*A*, blue) whose envelope (Fig. 1*A*, red) varied independently and more slowly in time. We initially focused on the electrosensory system of weakly electric fish because

Significance

We provide the first experimental evidence (to our knowledge) that correlated population activity can serve as an extra channel to encode second-order features of sensory input in both the electrosensory and vestibular systems. Through further experiments and mathematical modeling, we show that such coding not only requires but is also optimally tuned to a nonzero level of variability. Finally, we demonstrate that only physiologically realistic decoding circuits that explicitly include the contributions of pairwise neural activity can reliably be used to reconstruct the envelope. Our results reveal new functional roles for correlated activity and neural variability that are generally applicable across systems and species.

Author contributions: K.E.C. and M.J.C. designed research; M.G.M., M.J., J.C., O.Á.-Á., and M.J.C. performed research; M.G.M., M.J., J.C., O.Á.-Á., and M.J.C. analyzed data; and M.G.M., M.J., K.E.C., and M.J.C. wrote the paper.

The authors declare no conflict of interest.

This article is a PNAS Direct Submission.

[1]M.G.M. and M.J. contributed equally to this work.

[2]To whom correspondence should be addressed. Email: maurice.chacron@mcgill.ca.

This article contains supporting information online at www.pnas.org/lookup/suppl/doi:10.1073/pnas.1418224112/-/DCSupplemental.

(i) its neural circuitry is well characterized (10); (ii) it is feasible to perform pairwise recordings from electroreceptor afferents in awake behaving animals (18); and (iii) noise stimuli closely mimic natural sensory signals encountered by these fish (11) as they routinely evoke behavioral responses (19). When we examined simultaneous recordings from afferent pairs, we found that spike trains were more similar when the envelope was high (Fig. 1*B*). We quantified this similarity using the correlation coefficient (*SI Materials and Methods*) and found strong covariation with the envelope (Fig. 1*C*, *Top*). We quantified the degree to which the envelope could be predicted from the correlation coefficient by computing the variance-accounted-for (VAF) (*SI Materials and Methods* and *Materials and Methods*), which ranges between 0 (no predictability) and 1 (optimal predictability). The high VAF value (0.76) obtained indicates that the correlation coefficient is a reliable predictor of the envelope (Fig. 1*C*, *Bottom*).

Importantly, the activity of individual single neurons did not provide detailed information about the envelope (Fig. 1*D*, *Top*). Indeed, the cross-correlation function between the single electroreceptor's spiking activity and the envelope was not significantly different from that obtained from surrogate data that was, by construction, uncorrelated with the envelope ($P > 0.3$, Kolmogorov–Smirnov test; $n = 32$) (Fig. 1*D*, *Top*, *Inset*). We further found that standard nonlinear transformations that are typically used to extract the envelope from a signal also did not provide detailed information about the envelope when applied to the single electroreceptor neurons (Fig. 1*D*, *Bottom*). Overall, the pairwise correlation coefficient reliably predicted the envelope as quantified by a high VAF observed across our dataset (Fig. 1*E*). Similar results were obtained when randomly pairing nonsimultaneous recordings (Fig. 1*E*), indicating that such coding is robust. This is discussed further below. In contrast, waveforms obtained by applying either linear or nonlinear transformations to the single-neuron activity did not reliably predict the envelope as quantified by negligible VAF values (Fig. 1*E*).

We next investigated whether the value of the time window over which both the time-dependent correlation coefficient and firing rate are computed influences envelope-coding performance. This is because correlations reflecting common activity can be measured at different timescales, ranging from a few milliseconds (i.e., synchrony) to seconds (i.e., slow covariation of firing rates) (20). We found that the correlation coefficient provided detailed information about the envelope for integration time windows >1 s (Fig. 1*E*, *Inset*). However, for all time windows, single-neuron activity did not reliably predict the envelope, as quantified by negligible VAF values (Fig. 1*E*, *Inset*). Importantly, the time windows considered are comparable with neuronal integration time constants observed experimentally (21, 22).

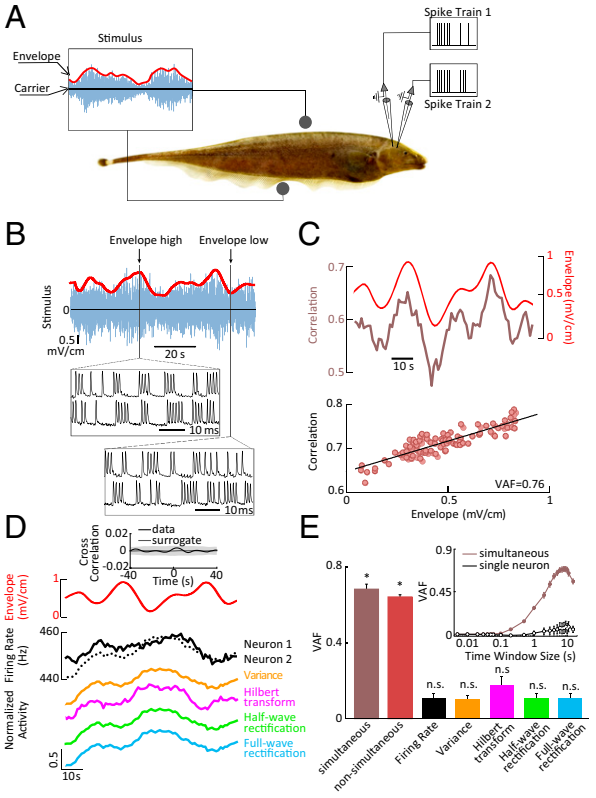

Fig. 1. Correlated but not single-neuron activity encodes the stimulus envelope in weakly electric fish electroreceptor afferents. (*A*) Electroreceptor afferents were stimulated with a noisy waveform (20-Hz cutoff frequency) (blue) whose amplitude (i.e., envelope, red) varied independently and consisted of low-pass–filtered white noise (0.05-Hz cutoff frequency). (*B*) Time-varying stimulus (blue) with zero mean (horizontal black line) and its envelope (red). (*Insets*) Spiking responses from an example afferent pair to stimulus segments characterized by high and low envelopes. Note that, although the total numbers of spikes were similar in both conditions (21 for high envelope vs. 23 for low envelope), coincident spikes were more frequent when the envelope was high (15 for high envelope vs. 8 for low envelope). (*C*, *Top*) Time-varying envelope (red), and correlation coefficient (brown) from the same pair. (*Bottom*) Correlation coefficient as a function of envelope showing a strong linear relationship as characterized by a high variance-accounted-for (VAF). (*D*, *Top*) Time-varying envelope (red), and corresponding firing rates of both neurons (black). (*Bottom*) Signals obtained after applying nonlinear transformations to the single-neuron activity. (*Inset*) Cross-correlation function between the envelope and an example single electroreceptor neuron's spiking activity (solid black) as well as uncorrelated surrogate data (solid gray). The band shows the 95% confidence interval of the surrogate dataset. (*E*) Population-averaged VAF values for the correlation coefficient computed from simultaneous recordings (brown; $n = 16$ pairs), nonsimultaneous recordings (red; $n = 153$), as well as for single-neural activity after applying either no transformation or the same nonlinear transformations as in *D* (black and colored bars; $n = 32$). No significant difference in coding performance as quantified by VAF was observed ($P = 0.12$, rank sum test, df = 168). The asterisk (*) indicates statistical significance at the $P = 0.01$ level using a Wilcoxon rank sum test. n.s., not statistically significant. (*Inset*) VAF computed from correlated activity of pairs of afferents recorded simultaneously and from single-neuron activity as a function of the time window used to calculate the correlation coefficient. The filled circles indicate statistically significant values from zero at the $P = 0.05$ level using a t test. The open circles indicate that the values were not significantly different from zero.

Envelope Coding by Correlated Activity in Leaky Integrate-and-Fire Neuron Models. Our results thus far lead to the interesting question: how does correlated activity encode the envelope? To answer this question, we simulated a pair of spiking neuron models using the leaky integrate-and-fire formalism. The inputs to both model neurons consisted of a constant bias current I_{bias}, a common stimulus $S(t)$ with zero mean and SD σ_{stim}, and normally distributed noise sources $\xi_1(t)$, $\xi_2(t)$ with zero mean and SD σ_{noise} (Fig. 2*A*, *SI Materials and Methods*). The output spike trains of our model neurons were analyzed in the same manner as the experimental data. We assumed that the noises received by each of the model neurons [i.e., $\xi_1(t)$, $\xi_2(t)$] were independent and identically distributed [$<\xi_i(t)\xi_j(t')> \propto \delta(t - t')$ if $i = j$ and $<\xi_i(t)\xi_j(t')> = 0$ otherwise]. Despite its relative simplicity and the fact that the patterns of the simulated neuron spike trains were different from those of electroreceptors (compare Figs. 1*B* and 2*B*), our model was able to accurately reproduce our experimental results (Fig. 2*B*). Specifically, the degree of similarity between both model neurons' spiking responses increased as a function of the envelope (Fig. 2*B*, compare *Middle* and *Bottom*). This can be understood intuitively because, although the noise intensity is independent of the envelope, the stimulus intensity and thus the signal-to-noise ratio is larger when the envelope is higher. Consistent with our experimental findings (Fig. 1*C*), the

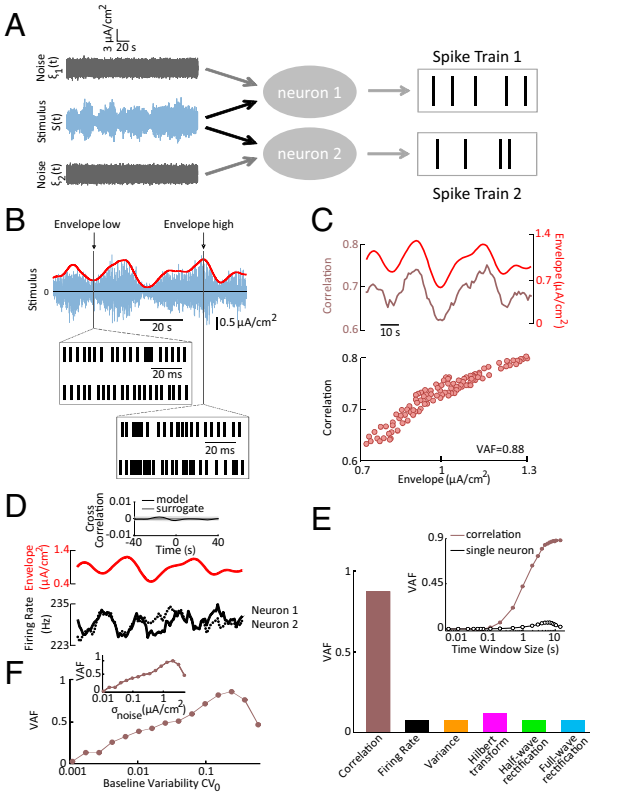

Fig. 2. An integrate-and-fire type neuron model predicts that correlated-based coding of envelopes is optimal for a nonzero level of neural variability. (*A*) Two leaky integrate-and-fire neurons received a common stimulus $S(t)$ (blue) as well as two independent noise sources $\xi_1(t)$, $\xi_2(t)$ (gray). (*B*) Time-varying stimulus (blue) with zero mean (horizontal black line) and its envelope (red). (*Insets*) Spiking responses to a stimulus segment characterized by a high and low envelope. (*C*, *Top*) Time-varying envelope (red), and correlation coefficient (brown) from our pair of model neurons. (*Bottom*) Correlation coefficient as a function of envelope showing a strong linear relationship as characterized by a high variance-accounted-for (VAF). (*D*, *Top*) Time-varying envelope (red), and corresponding firing rates of the single model neurons (*Bottom*; black). (*Inset*) Cross-correlation function between the envelope and our single model neuron's spiking activity (solid black) as well as uncorrelated surrogate data (solid gray). The band shows the 95% confidence interval of the surrogate dataset. (*E*) VAF values for correlation coefficient as well as for single neural activity after applying either no transformation or the same nonlinear transformations as in *D*. (*Inset*) VAF computed from correlated activity of pairs of model neurons and from single-neuron activity as a function of the time window used to calculate the correlation coefficient. Abbreviations are the same as in Fig. 1. (*F*) VAF computed from the correlation coefficient as a function of variability as quantified by the coefficient of variation from the baseline activity CV_0. Different values of CV_0 were obtained by varying the noise intensity σ_{noise} in our model between 0.1 and 20 μA/cm². (*Inset*) VAF as a function of noise intensity σ_{noise}.

pairwise correlation coefficient reliably predicted the envelope as quantified by a high VAF (Fig. 2*C*). In contrast, individual single-model neuron activity did not provide detailed information about the envelope (Fig. 2*D*). Indeed, the cross-correlation function between the single model neuron's spiking activity and the envelope was not significantly different from zero ($P > 0.3$, Kolmogorov–Smirnov test) (Fig. 2*D*, *Top*, *Inset*). The signals obtained by applying nonlinear transformations to the single-model neuron activity also could not reliably predict the envelope as quantified by negligible VAF values (Fig. 2*E*). Furthermore, as was the case experimentally, the correlation coefficient most reliably predicted the envelope when computed for time windows > 1 s (compare *Insets* of Figs. 1*E* and 2*E*).

To test whether envelope coding by correlated but not single-neuron activity is robust in our model, we next systematically varied parameters such as the bias current I_{bias}, the stimulus intensity σ_{stim}, and the noise intensity σ_{noise}. We found that correlated population activity encoded the envelope independently of single-neuron activity over a wide range of parameter values. Specifically, this was the case for higher values of I_{bias} as well as intermediate values of σ_{stim} and σ_{noise} (Figs. S1*A* and S2*A*). Furthermore, we found that the stimulus input–firing-rate output relationship was approximately linear in this regime (Figs. S1*B* and S2*B*). In contrast, single-neuron activity could only predict the envelope for regions in parameter space (Figs. S1*A* and S2*B*) that were characterized by a nonlinear stimulus input–firing-rate output relationship (Figs. S1*B* and S2*B*) (*SI Materials and Methods*, *Model Simulations*).

Our model also makes the unexpected prediction that envelope coding by correlated neural activity requires neural variability as quantified by either the noise intensity σ_{noise} or the coefficient of variation of the baseline (i.e., in the absence of stimulation) activity CV_0. Both quantities are strongly correlated with trial-to-trial variability in the neural response to repeated presentations of the stimulus (18, 23, 24). We found that the VAF between correlation coefficient and envelope was maximal for a nonzero value of CV_0 (Fig. 2*F*) and σ_{noise} (Fig. 2*F*, *Inset*). Intuitively this makes sense because both infinitesimally small and infinitely large values of CV_0 or σ_{noise} give rise to regimes where the correlation coefficient is always equal to zero and unity, respectively, and thus independent of the envelope.

Envelope Coding by Correlated Vestibular Afferent Activities. Our modeling and associated analyses have made the important prediction that envelope coding by correlated activity is optimal for a nonzero level of neuronal variability. To test this prediction experimentally, we recorded from afferents in the primate vestibular system (Fig. 3*A*; *SI Materials and Methods*). These afferents are particularly well suited because they display a much wider range of variability than that observed for electroreceptor afferents (12, 15), which is due in part to distinct ionic conductances and morphological features at their peripheral terminations (25).

We first investigated whether vestibular afferents display envelope coding by correlated activity. The waveform and envelope of motion stimuli (Fig. 3*A*; *SI Materials and Methods*) resembled vestibular signals encountered in a naturalistic setting (17). We obtained results that were qualitatively similar to those described above for the electrosensory system: spiking responses from pairs of single vestibular afferents were more similar when the envelope was high (Fig. 3*B*, compare *Middle* and *Bottom*) and the correlation coefficient between pairs of vestibular afferents strongly covaried with the envelope waveform as quantified by a large VAF (Fig. 3*C*). Furthermore, as seen in Fig. 3*D*, neither linear nor nonlinear transformations applied to the single-afferent activity gave detailed information about the envelope signal as quantified by negligible VAFs (Fig. 3*E*). Moreover, the cross-correlation function between the single afferent's spiking activity and the envelope was not significantly different from zero ($P > 0.3$, Kolmogorov–Smirnov test; $n = 18$) (Fig. 3*D*, *Top*, *Inset*). Finally, we found that the correlation coefficient most reliably predicted the envelope for relatively large (>1 s) time windows (Fig. 3*E*, *Inset*). Thus, correlated but not single vestibular afferent activity encodes the envelope in a manner similar to that observed for electroreceptor afferents and our model.

Envelope Coding by Correlated Activity Is Optimal for a Nonzero Level of Neural Variability. Next, to test our model's prediction that envelope coding by correlated activity is optimally tuned to a nonzero level of neural variability, we plotted the coding efficiency as a function of variability quantified from baseline activity (i.e., in the absence of stimulation) for pairs of vestibular afferents.

NEUROSCIENCE

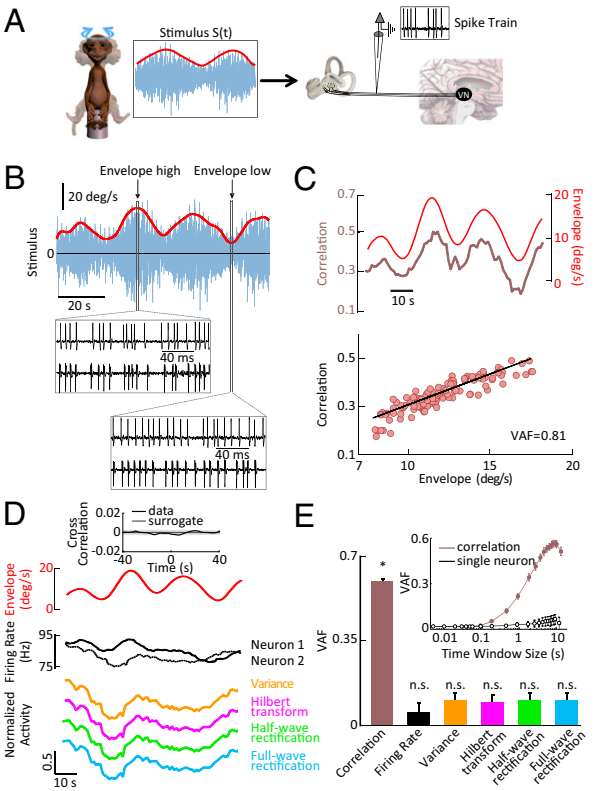

Fig. 3. Correlated but not single-neuron activity encodes the stimulus envelope in primate vestibular afferents. (*A*) The spiking activity of individual vestibular afferents were recorded from macaque monkeys during rotational stimuli whose angular velocity consisted of a noisy waveform (20-Hz cutoff frequency) (blue) whose amplitude (i.e., envelope, red) varied independently and consisted of low-pass–filtered white noise (0.05-Hz cutoff frequency). (*B*) Time-varying stimulus (blue) with zero mean (horizontal black line) and its envelope (red). (*Insets*) Spiking responses from an example vestibular afferent pair to a stimulus segment characterized by a high and low envelope. Note that, although the total numbers of spikes were similar (~21), coincident spikes were more frequent when the envelope was high (16 vs. 9). (*C*, *Top*) Time-varying envelope (red), and correlation coefficient (brown) from the same pair. (*Bottom*) Correlation coefficient as a function of envelope showing a strong linear relationship as characterized by a high variance-accounted-for (VAF). (*D*, *Top*) Time-varying envelope (red), and corresponding firing rates of both neurons (black). (*Bottom*) Single-neural activity after applying nonlinear operations as in Fig. 1. (*Inset*) Cross-correlation function between the envelope and an example single vestibular afferent's spiking activity (solid black) as well as uncorrelated surrogate data (solid gray). The band shows the 95% confidence interval of the surrogate dataset. (*E*) Population-averaged VAF values for correlation coefficient (red; $n = 121$ pairs), as well as for firing rate and for single-neural activity after applying nonlinear operations (black and colored bars; $n = 18$). The asterisk (*) indicates statistical significance at the $P = 0.01$ level using a Wilcoxon rank sum test. (*Inset*) VAF computed from correlated activity of reconstituted pairs of afferents and from single-neuron activity as a function of the time window used to calculate the correlation coefficient. Filled circles indicate statistically significant values from zero at the $P = 0.05$ level using a t test. Open circles indicate that the values were not significantly different from zero.

Confirming our modeling prediction, the largest VAF values were seen for vestibular afferent pairs with intermediate levels of variability (Fig. 4*A*, green circles). Even more strikingly, superimposing data obtained from electroreceptor afferent pairs revealed that vestibular and electroreceptor afferent pairs with similar levels of variability also display similar VAFs (Fig. 4*A*, compare black and green circles). This marked overlap between the datasets from both sensory systems given important differences (12, 15). Furthermore, we found that our model could reproduce the experimentally observed relationship between coding efficiency and neural variability seen in both datasets (Fig. 4*A*, compare stars with black and green circles). Thus, our results suggest that the same relationship between the efficiency of envelope coding by correlated activity and neural variability is shared across sensory systems and species.

Decoding Information About Second-Order Stimulus Attributes Carried by Neural Correlations. The results above demonstrate that correlated neural activity reliably encodes second-order sensory information. However, information carried by neural activity is only useful to an organism if it is actually decoded by higher-order

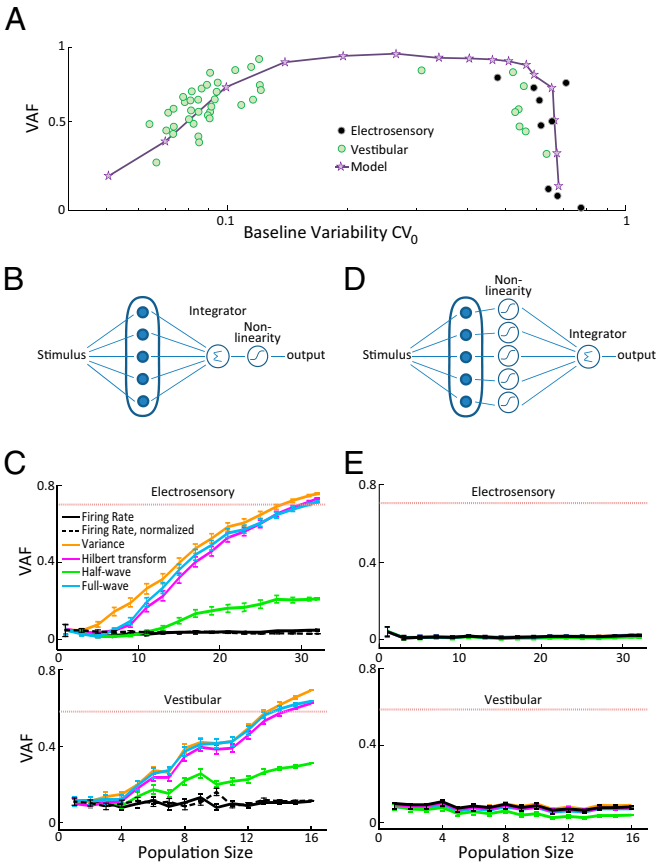

Fig. 4. Can the brain decode information carried by correlated neural activity? (*A*, *Top*) VAF obtained from the correlation coefficient as a function of baseline variability defined as the geometric mean of the coefficient of variations for pairs of electroreceptor afferents (black circles), vestibular afferents (green circles), and variability defined as CV_0 from our model (purple stars) when we covaried both noise intensity and bias current (*SI Materials and Methods*). We note that there are few data points in the intermediate variability range: this is most likely because the probability of finding vestibular afferents in this range is relatively low (15, 42). (*B*) Schematic of a physiologically realistic decoder for which the individual afferent neuron's activities are first averaged before applying a nonlinear transformation. (*C*) Performance of the decoder described in *B* quantified by VAF as a function of population size for the electrosensory (*Top*) and the vestibular (*Bottom*) dataset. The population-averaged value obtained from the correlation coefficient from neuron pairs is also shown (dashed red line) for comparison. (*D*) Schematic of a decoder based on applying a nonlinear transformation on each individual neuron's spiking before averaging. (*E*) Performance of the decoder described in *D* quantified by VAF as a function of the number of afferents for the electrosensory (*Top*) and the vestibular (*Bottom*) dataset. The population-averaged value obtained from the correlation coefficient obtained from neuron pairs is also shown (dashed red line) for comparison.

brain areas. To test whether information about the envelope can actually be decoded, we considered a neural circuit for which the output is a nonlinear function of the summed activities of single neurons (Fig. 4*B*). Because downstream neurons nonlinearly integrate input from convergent afferent axons in both the electrosensory and vestibular systems (16, 26), this circuit effectively functions as a physiologically realistic decoding algorithm. Indeed, we found that this circuit's decoding performance improved with increasing population size using several standard nonlinear functions (Fig. 4*C*, *Top* and *Bottom*, colored traces). In contrast, linear summation of the single-neuron activities alone led to poor performance that did not improve with increasing population size (Fig. 4*C*, solid black). Similar results were obtained when linearly summing the normalized (i.e., subtracting the mean value and dividing by the maximum value) single-neuron activities (Fig. 4*C*, dashed black). Thus, nonlinear integration is necessary to observe improved decoding performance with increasing population size.

The neural circuit considered above (Fig. 4*B*) explicitly includes the contributions of pairwise interactions between neurons (i.e., "cross-terms") toward decoding information about the envelope because the nonlinear transformation is applied after summation (*SI Materials and Methods*). However, the observed improvement in performance in this circuit could have been due to simple averaging the variability over a neural population. To address this possibility, we considered an alternate neural circuit in which a nonlinear operation is first performed on each individual neuron's spiking activity followed by summing (Fig. 4*D*). Unlike the neural circuit considered in Fig. 4*B*, this circuit does not take into account joint statistics because the nonlinear transformation is applied before summation (*SI Materials and Methods*). Thus, if the improvement in performance observed in Fig. 4*C* was due to simple averaging, then we should observe an improvement in performance with increasing population size similar to that seen in Fig. 4*C*. If, on the other hand, the improvement in performance was instead due to taking into account joint statistics, then we should observe poor performance that does not improve with increasing population size. We found that the performance of this latter decoding algorithm was poor and did not significantly improve with increasing population size (Fig. 4*E*), thereby showing that taking into account pairwise joint statistics between neural spike trains is necessary to recover information about second-order stimulus attributes.

Discussion

We investigated the responses of both fish electrosensory and primate vestibular afferents to naturalistic stimuli. In both systems, we found that pairwise correlated but not single-neuron activity provided detailed information about the second-order attributes of the stimulus (i.e., the envelope). Through a combination of modeling and theoretical analyses, we predicted that this coding is optimal for a nonzero level of neural variability. We validated this prediction experimentally and found that both electrosensory and vestibular neurons were described by the same tuning function relating coding efficiency to neural variability. Finally, we found that the envelope information contained in correlated neural activity can only be decoded when joint statistics are taken into account. Taken together, our results suggest that envelope coding by correlated activity is a general strategy used across sensory systems and species to transmit information about behaviorally relevant stimulus attributes.

Correlated neural activities have been observed ubiquitously in the central nervous system (2), and it is now well accepted that their structure is dynamically regulated by several factors (27–31). This has led to the interesting hypothesis that correlated activity carries information not found in single-neuron activity (31, 32). Indeed, our results provide an experimental demonstration of this phenomenon by showing that correlated but not single-neuron activity transmits information about a behaviorally relevant stimulus feature. Traditionally, neural correlations have been separated into signal (i.e., correlations between the average neural responses) and noise (i.e., correlations between neural variabilities) components. Here, we showed that correlation coding by correlated activity was similar when using either simultaneous or nonsimultaneous recordings. Our findings thus demonstrate that signal correlations carry envelope information. Importantly, the structure of noise correlations can strongly depend on the stimulus' spatiotemporal frequency content (28, 33). These results suggest that noise correlations carry information that may not be found in single-neuron activity, but further studies in other brain areas are needed to test this interesting hypothesis.

Across sensory systems, natural stimuli tend to display prominent first- and second-order attributes that are critical for perception (5, 7, 34, 35). In the electrosensory system, second-order attributes carry important information about the relative distance between conspecifics (11). It is likely that higher brain areas decode information about second-order attributes carried by correlated electroreceptor activity because weakly electric fish display strong and reliable behavioral responses to these attributes (13). Indeed, pyramidal cells within the electrosensory lateral line lobe strongly respond to envelopes at the single-neuron level (36) presumably through nonlinear integration of afferent synaptic input (26). In the vestibular system, neurons within the vestibular nuclei also nonlinearly integrate convergent vestibular afferent input (16) and are thus expected to strongly respond to the envelopes found in natural vestibular stimuli (17). However, further studies are needed to test these important predictions.

Our results have shown that neural variability is necessary to observe envelope coding by correlated neural activity. The role of neural variability in sensory coding has been the focus of much debate (1). On the one hand, the common wisdom is that variability is an unavoidable consequence of having neurons interconnected and should then be minimized (e.g., by pooling neural activities) to mitigate detrimental effects on neural coding. The vestibular system is uniquely well suited to study the role of variability in coding because afferents display a wide range of resting discharge variability. Interestingly, hair cells giving rise to vestibular afferents with high resting discharge variability can only be found in amniotes. It is, furthermore, thought that their recent evolution was triggered by changes in vestibular stimulus statistics resulting from transitioning from an aquatic to a terrestrial environment (37), which is incompatible with the above point of view that variability is detrimental to neural coding. Alternatively, it has been more recently postulated that neural variability instead forms a key element of the neural code by promoting increased information transmission (1). Indeed, theoretical studies posit that trial-to-trial variability in the neural response can effectively increase information transmission (38). Our results showing that correlated activity can optimally transmit information about the envelope for a nonzero level of variability provide a novel beneficial role for neural variability in sensory coding.

We note that, when the relationship between the stimulus waveform input and the firing-rate output is nonlinear, single-neuron activity can provide detailed information about the envelope as previously observed (8, 9, 39). Response nonlinearities (e.g., rectification, phase-locking) are more likely to be elicited by stimuli with relatively large intensities (40–42). However, natural stimuli are usually characterized by relatively low intensities yet can give rise to robust behavioral responses (13, 17, 43, 44). In these conditions, our results show that single-neuron activity instead does not provide detailed information about the envelope.

Thus, we propose that the coding of low-amplitude envelopes by correlated but not single-neuron activity is a general feature of sensory processing. Our results show that, in this regime, correlated but not single-neuron activity can provide detailed information about the envelope that can be recovered by pooling

neural activities before performing a nonlinear transformation. We speculate that envelope coding by correlated activity will be preferentially found in neurons that display relatively high levels of spontaneous activity because these neurons tend to respond to low-intensity slowly time-varying stimuli through linearly related changes in activity around the spontaneous level. Such neurons can be found throughout the brain including cortex (15, 45–47). It is thus very likely that, across species, other sensory systems use similar decoding strategies that take advantage of the fact that correlated activity carries information about distinct stimulus attributes such as the envelope to ensure accurate perception and behavioral responses.

Materials and Methods

A detailed description of the methods is provided in *SI Materials and Methods*. All procedures were approved by the McGill University's Animal Care Committee and were in compliance with the guidelines of the Canadian Council on Animal Care. In brief, recordings from electrosensory and vestibular afferents were obtained using standard techniques. Spike trains were recorded in response to stimuli $S(t)$ lasting 120 s and consisting of a 0- to 20-Hz noise carrier whose amplitude (i.e., envelope) was modulated independently (0–0.05 Hz). Correlations were quantified using the correlation coefficient. Variability was quantified by computing the coefficient of variation of the baseline activity (i.e., in the absence of stimulation), CV_0, which is strongly correlated with trial-to-trial variability in the neural response to repeated stimulus presentations (18, 23, 24). VAF was used to assess the ability of a given time-varying signal to predict the envelope. Unless otherwise indicated, all error bars indicate SEs, and all statistical tests were Wilcoxon rank sum tests, except where stated otherwise. Our model consisted of two neurons receiving a common stimulus $S(t)$ with intensity σ_{stim} as well as independent and identically distributed Gaussian white-noise sources with intensity σ_{noise}. Simulations shown in Fig. 2 were obtained using $\sigma_{noise} > \sigma_{stim}$, and model spike trains were analyzed in the same way as the experimental data.

ACKNOWLEDGMENTS. We thank L. Maler for critical reading of the manuscript. This research was supported by the Canadian Institutes of Health Research (M.J.C. and K.E.C.) and the National Institutes of Health (K.E.C.).

1. Stein RB, Gossen ER, Jones KE (2005) Neuronal variability: Noise or part of the signal? *Nat Rev Neurosci* 6(5):389–397.
2. Averbeck BB, Latham PE, Pouget A (2006) Neural correlations, population coding and computation. *Nat Rev Neurosci* 7(5):358–366.
3. Hong S, Ratté S, Prescott SA, De Schutter E (2012) Single neuron firing properties impact correlation-based population coding. *J Neurosci* 32(4):1413–1428.
4. Faisal AA, Selen LP, Wolpert DM (2008) Noise in the nervous system. *Nat Rev Neurosci* 9(4):292–303.
5. Shannon RV, Zeng FG, Wygonski J (1998) Speech recognition with altered spectral distribution of envelope cues. *J Acoust Soc Am* 104(4):2467–2476.
6. Bertoncini J, Serniclaes W, Lorenzi C (2009) Discrimination of speech sounds based upon temporal envelope versus fine structure cues in 5- to 7-year-old children. *J Speech Lang Hear Res* 52(3):682–695.
7. Stamper SA, Fortune ES, Chacron MJ (2013) Perception and coding of envelopes in weakly electric fishes. *J Exp Biol* 216(Pt 13):2393–2402.
8. Fairhall AL, Lewen GD, Bialek W, de Ruyter Van Steveninck RR (2001) Efficiency and ambiguity in an adaptive neural code. *Nature* 412(6849):787–792.
9. Lundstrom BN, Fairhall AL, Maravall M (2010) Multiple timescale encoding of slowly varying whisker stimulus envelope in cortical and thalamic neurons in vivo. *J Neurosci* 30(14):5071–5077.
10. Chacron MJ, Longtin A, Maler L (2011) Efficient computation via sparse coding in electrosensory neural networks. *Curr Opin Neurobiol* 21(5):752–760.
11. Fotowat H, Harrison RR, Krahe R (2013) Statistics of the electrosensory input in the freely swimming weakly electric fish *Apteronotus leptorhynchus*. *J Neurosci* 33(34): 13758–13772.
12. Gussin D, Benda J, Maler L (2007) Limits of linear rate coding of dynamic stimuli by electroreceptor afferents. *J Neurophysiol* 97(4):2917–2929.
13. Metzen MG, Chacron MJ (2014) Weakly electric fish display behavioral responses to envelopes naturally occurring during movement: Implications for neural processing. *J Exp Biol* 217(Pt 8):1381–1391.
14. Cullen KE (2011) The neural encoding of self-motion. *Curr Opin Neurobiol* 21(4): 587–595.
15. Goldberg JM (2000) Afferent diversity and the organization of central vestibular pathways. *Exp Brain Res* 130(3):277–297.
16. Massot C, Schneider AD, Chacron MJ, Cullen KE (2012) The vestibular system implements a linear-nonlinear transformation in order to encode self-motion. *PLoS Biol* 10(7):e1001365.
17. Carriot J, Jamali M, Chacron MJ, Cullen KE (2014) Statistics of the vestibular input experienced during natural self-motion: Implications for neural processing. *J Neurosci* 34(24):8347–8357.
18. Chacron MJ, Maler L, Bastian J (2005) Electroreceptor neuron dynamics shape information transmission. *Nat Neurosci* 8(5):673–678.
19. Chacron MJ, Doiron B, Maler L, Longtin A, Bastian J (2003) Non-classical receptive field mediates switch in a sensory neuron's frequency tuning. *Nature* 423(6935): 77–81.
20. Litwin-Kumar A, Oswald AMM, Urban NN, Doiron B (2011) Balanced synaptic input shapes the correlation between neural spike trains. *PLoS Comput Biol* 7(12):e1002305.
21. Cannon SC, Robinson DA (1987) Loss of the neural integrator of the oculomotor system from brain stem lesions in monkey. *J Neurophysiol* 57(5):1383–1409.
22. Prescott SA, De Koninck Y (2005) Integration time in a subset of spinal lamina I neurons is lengthened by sodium and calcium currents acting synergistically to prolong subthreshold depolarization. *J Neurosci* 25(19):4743–4754.
23. Chacron MJ, Longtin A, Maler L (2003) The effects of spontaneous activity, background noise, and the stimulus ensemble on information transfer in neurons. *Network* 14(4):803–824.
24. Yu XJ, Thomassen JS, Dickman JD, Newlands SD, Angelaki DE (2014) Long-term deficits in motion detection thresholds and spike count variability after unilateral vestibular lesion. *J Neurophysiol* 112(4):870–889.
25. Eatock RA, Hurley KM (2003) Functional development of hair cells. *Curr Top Dev Biol* 57:389–448.
26. Berman NJ, Maler L (1999) Neural architecture of the electrosensory lateral line lobe: Adaptations for coincidence detection, a sensory searchlight and frequency-dependent adaptive filtering. *J Exp Biol* 202(Pt 10):1243–1253.
27. Cohen MR, Maunsell JH (2009) Attention improves performance primarily by reducing interneuronal correlations. *Nat Neurosci* 12(12):1594–1600.
28. Chacron MJ, Bastian J (2008) Population coding by electrosensory neurons. *J Neurophysiol* 99(4):1825–1835.
29. Vaadia E, et al. (1995) Dynamics of neuronal interactions in monkey cortex in relation to behavioural events. *Nature* 373(6514):515–518.
30. Litwin-Kumar A, Chacron MJ, Doiron B (2012) The spatial structure of stimuli shapes the timescale of correlations in population spiking activity. *PLoS Comput Biol* 8(9): e1002667.
31. deCharms RC, Merzenich MM (1996) Primary cortical representation of sounds by the coordination of action-potential timing. *Nature* 381(6583):610–613.
32. Ishikane H, Gangi M, Honda S, Tachibana M (2005) Synchronized retinal oscillations encode essential information for escape behavior in frogs. *Nat Neurosci* 8(8):1087–1095.
33. Ponce-Alvarez A, Thiele A, Albright TD, Stoner GR, Deco G (2013) Stimulus-dependent variability and noise correlations in cortical MT neurons. *Proc Natl Acad Sci USA* 110(32):13162–13167.
34. Joris PX, Schreiner CE, Rees A (2004) Neural processing of amplitude-modulated sounds. *Physiol Rev* 84(2):541–577.
35. Baker CL, Jr (1999) Central neural mechanisms for detecting second-order motion. *Curr Opin Neurobiol* 9(4):461–466.
36. McGillivray P, Vonderschen K, Fortune ES, Chacron MJ (2012) Parallel coding of first- and second-order stimulus attributes by midbrain electrosensory neurons. *J Neurosci* 32(16):5510–5524.
37. Eatock RA, Songer JE (2011) Vestibular hair cells and afferents: Two channels for head motion signals. *Annu Rev Neurosci* 34:501–534.
38. McDonnell MD, Ward LM (2011) The benefits of noise in neural systems: Bridging theory and experiment. *Nat Rev Neurosci* 12(7):415–426.
39. Rosenberg A, Issa NP (2011) The Y cell visual pathway implements a demodulating nonlinearity. *Neuron* 71(2):348–361.
40. Savard M, Krahe R, Chacron MJ (2011) Neural heterogeneities influence envelope and temporal coding at the sensory periphery. *Neuroscience* 172:270–284.
41. Metzen MG, Chacron MJ (2015) Neural heterogeneities determine response characteristics to second-, but not first-order stimulus features. *J Neurosci* 35(7):3124–3138.
42. Sadeghi SG, Minor LB, Cullen KE (2007) Response of vestibular-nerve afferents to active and passive rotations under normal conditions and after unilateral labyrinthectomy. *J Neurophysiol* 97(2):1503–1514.
43. Simoncelli EP, Olshausen BA (2001) Natural image statistics and neural representation. *Annu Rev Neurosci* 24:1193–1216.
44. Deemyad T, Metzen MG, Pan Y, Chacron MJ (2013) Serotonin selectively enhances perception and sensory neural responses to stimuli generated by same-sex conspecifics. *Proc Natl Acad Sci USA* 110(48):19609–19614.
45. Kuffler SW (1953) Discharge patterns and functional organization of mammalian retina. *J Neurophysiol* 16(1):37–68.
46. Luczak A, Barthó P, Harris KD (2009) Spontaneous events outline the realm of possible sensory responses in neocortical populations. *Neuron* 62(3):413–425.
47. Arieli A, Sterkin A, Grinvald A, Aertsen A (1996) Dynamics of ongoing activity: Explanation of the large variability in evoked cortical responses. *Science* 273(5283): 1868–1871.

Supporting Information

Metzen et al. 10.1073/pnas.1418224112

SI Materials and Methods

Animals and Recording.

Electrosensory system. We gathered data from five adult *Apteronotus leptorhynchus*. The animals were acquired from local tropical fish suppliers and were housed in groups (2–10) at controlled water temperature (26–29 °C) and conductivity (300–800 μS/cm) and a 12:12-h dark:light cycle according to published guidelines (1). Before surgery, animals were paralyzed with an intramuscular injection of tubocurarine chloride hydrate (1 μg/g body weight of a 0.2% solution; Sigma). Surgical methods have been previously described in detail (2–8). In brief, animals were transferred to an experimental tank (30 cm × 30 cm × 10 cm) containing water from the animal's home tank and respired by a constant flow of oxygenated water through their mouth. The animal's head was then locally anesthetized with lidocaine ointment (5%; AstraZeneca). Subsequently, the skull was partly exposed and a small window was opened over the recording region.

Sharp glass micropipette electrodes (20–50 MΩ) backfilled with 3 M KCl were used to record simultaneously in vivo from pairs of P-type electrosensory afferent axons (P-units) in the deep-fiber layer of the electrosensory lateral line lobe (ELL). In general, recording from P-units were done as described in previous studies (9, 10). P-units can be easily identified as their probability of firing increases with increasing EOD amplitude (11). The recording electrodes were advanced into the ELL with a piezoelectric microdrive (Inchworm, IW-711; Kopf) for one P-unit, and manually with a one-axis oil hydraulic micromanipulator (type MO-10; Narishige) for the second P-unit. The recorded potentials were amplified (Duo 773 Electrometer; World Precision Instruments), digitized at 10-kHz sampling rate each using CED 1401plus hardware and Spike2 software (Cambridge Electronic Design), and stored on a computer hard disk for offline analysis. The EOD was recorded between the head and tail of the fish by using two vertical metal wires, amplified (model 1700 amplifier; A-M Systems; bandpass filter between 300 Hz and 5 kHz) and digitized at 10 kHz using a CED Power1401 with Spike2 software (Cambridge Electronic Design).

Vestibular system. We also gathered data from two adult male macaque monkeys (*Macaca fascicularis*). Monkeys were housed in pairs and kept on a 12:12-h dark:light cycle. They were prepared for chronic extracellular recording using aseptic surgical techniques. The surgical preparation was similar to that previously described (12). Briefly, using aseptic surgical techniques and under isoflurane anesthesia (0.8–1.5%), a stainless-steel post was secured to the animal's skull with stainless-steel screws and dental acrylic resin, allowing complete immobilization of the head during the experiments. The implant also held in place a recording chamber oriented stereotaxically toward the vestibular nerve where it emerges from the internal auditory meatus. Finally, an 18- to 19-mm-diameter eye coil (three loops of Teflon-coated stainless-steel wire) was implanted in the right eye behind the conjunctiva. After the surgery, buprenorphine (0.01 mg/kg, i.m.) was administered as postoperative analgesia every 12 h for 2–5 d depending on the animal's pain level, and Anafen (2 mg/kg, then 1 mg/kg subsequent days) was used as an antiinflammatory. In addition, cefazolin (25 mg/kg, i.m.) was injected twice daily for 10 d. Animals were given at least 2 wk to recuperate from the surgery before any experiments began.

During the experiment, the head-restrained monkey was seated in a primate chair mounted on top of a vestibular turntable in a dimly lit room. The vestibular nerve was approached through the floccular lobe of the cerebellum, as identified by its eye movement-related activity (13–15); entry to the nerve was preceded by a silence, indicating that the electrode had left the cerebellum. Extracellular single-unit activity of semicircular canal afferents was recorded using glass microelectrodes (24–27 MΩ), the depth of which was controlled using a precision hydraulic microdrive (Narishige). Rotational head velocity was measured using an angular velocity sensor (Watson) firmly secured to the animal's head post. During experimental sessions, unit activity, horizontal and vertical eye positions, and head velocity signals were recorded on digital audiotape for later playback. During playback, action potentials from extracellular recordings were discriminated using a windowing circuit (BAK Electronics). Eye position and head velocity signals were low-pass filtered at 250 Hz (eight-pole Bessel filter) and sampled at 1 kHz.

We confirmed that each unit discharged in a manner consistent with previous characterizations of the afferents that innervate the horizontal semicircular canals (16, 17). All afferents that were included in the present study responded to rotational head movements toward the side of the recording (i.e., ipsilateral yaw), but not in response to static tilts. In addition, we verified that responses were not modulated during saccadic or pursuit eye movements.

Stimulation.

Electrosensory system. The electrosensory stimuli used in this study consisted of amplitude modulations (AMs) of the animals own EOD. It is important to note that the EOD waveform itself, a quasisinusoidal signal, can be considered as a carrier signal and that the relevant stimulus here is the AM of this carrier signal (11). Therefore, we will henceforth refer to the AM as the stimulus $S(t)$. To obtain time-varying AMs of the fish's own EOD, the desired signal waveform was first multiplied (MT3 multiplier; Tucker- Davis Technologies) with a white-noise–modulated sinusoidal carrier wave that was phase-locked to the animal's own EOD. The resulting signal was then attenuated (Leader; LAT-45; Leader Electronics), isolated from ground (World Precision Instruments; A395 linear stimulus isolator), and delivered to the experimental tank via a pair of silver–silver chloride electrodes located ∼20 cm on each side of the animal. This stimulation configuration is referred to as "global" in previous studies, because the electric image caused by the stimulus covers most if not all of the animal's skin surface (6, 7, 18). The electrosensory stimuli used in this study resembled mimics of natural stimuli (19) and were given by the following:

$$S_{electrosensory}(t) = A_{electrosensory}\left[1 + \sigma_{electrosensory}\psi(t)\right]\zeta(t), \qquad \textbf{[S1]}$$

where $\zeta(t)$ and $\psi(t)$ are low-pass–filtered (eighth-order Butterworth; 20- and 0.05-Hz cutoff frequencies, respectively) Gaussian white noise processes with zero mean and SD unity, respectively. The depth of modulation $\sigma_{electrosensory}$ was set to 0.9, and the stimulus duration was 120 s. The stimulus intensity $A_{electrosensory}$ was adjusted such that the electroreceptor afferents did not show any nonlinear responses like saturation or rectification (20) and typically was 0.1–0.3 mV/cm. Note that, before electrosensory stimulation, each afferent's spontaneous activity (i.e., discharge in the absence of stimulation) was recorded for a minimum 20 s so that discharge variability could be quantified.

Vestibular system. The vestibular stimuli used in this study also resembled mimics of natural stimuli and consisted of rotational movements with angular velocities spanning a broad range of

frequencies. These had the same profile as the electrosensory stimuli and were also given by the following:

$$S_{vestibular}(t) = A_{vestibular}[1 + \sigma_{vestibular}\psi(t)]\zeta(t), \quad \textbf{[S2]}$$

where $\zeta(t)$ and $\psi(t)$ are low-pass–filtered (eighth-order Butterworth; 20- and 0.05-Hz cutoff frequencies, respectively) Gaussian white noise processes with zero mean and SD unity, respectively. The depth of modulation $\sigma_{vestibular}$ was set to 0.6, and the stimulus duration was 120 s. The stimulus intensity $A_{vestibular}$ during recordings was adjusted such as to avoid nonlinear responses like saturation or rectification (21) and was typically set to 40 deg/s. Note that, before vestibular stimulation, each afferent's spontaneous activity (i.e., discharge in the absence of head movement) was recorded for a minimum 20 s so that discharge variability could be quantified.

Data Analysis. All off-line analysis routines were custom written in Matlab (MathWork). Importantly, both vestibular and electrosensory data were analyzed in the same fashion. A sequence $R(t)$ was constructed from the spike times by setting the value of bin i to the number of spikes occurring within it. We varied the binwidth between 0.1 and 100 ms in our model and found that this did not significantly alter our estimates of the correlation coefficient (data not shown; see below). We thus used a binwidth of 1 ms for all presented results. We excluded neurons that were not robustly driven by the stimulus, which typically occurred because of poor isolation as determined by standard criteria (e.g., the presence of an absolute refractory period).

Extracting the stimulus envelope. The envelope can be regarded as the instantaneous amplitude of the stimulus $S(t)$, or its time-varying contrast. It can be obtained from the stimulus $S(t)$ by the following nonlinear transformation:

$$E(t) = \sqrt{S(t)^2 + \hat{S}(t)^2}, \quad \textbf{[S3]}$$

where $\hat{S}(t)$ is the Hilbert transform of $S(t)$ given by the following (22–24):

$$\hat{S}(t) = \frac{1}{\pi} C\left[\int_{-\infty}^{+\infty} \frac{S(\tau)}{t-\tau} d\tau\right], \quad \textbf{[S4]}$$

where C is the Cauchy principal value.

Computing correlation between the spiking activities of neurons. We computed the cross-correlation coefficient between the responses R_i and R_j of neurons i and j, which is defined by the following (25):

$$\rho = \frac{\int_{-\infty}^{+\infty} d\tau \langle \Delta R_i(t) \Delta R_j(t+\tau) \rangle}{\sqrt{\int_{-\infty}^{+\infty} d\tau \langle \Delta R_i(t) \Delta R_i(t+\tau) \rangle \int_{-\infty}^{+\infty} d\tau \langle \Delta R_j(t) \Delta R_j(t+\tau) \rangle}}, \quad \textbf{[S5]}$$

where $<\ldots>$ denotes an average over realizations or over time and $\Delta R_j(t) = R_j(t) - <R_j(t)>$. We note that this definition is slightly different from the one used in previous studies (26). These studies instead considered correlations between the spike counts computed over a given binwidth at zero lag. The relationship between both approaches has been described in detail elsewhere (27). In practice, we used a time window of 5 ms $\leq T \leq$ 15 s that was slid along the two binary sequences [$R_i(t)$ and $R_j(t)$] of the two neurons in time steps of $dT \leq 1$ s. In each time window T_k, the coherence between the two binary sequences [$R_i(t)$ and $R_j(t)$] was computed by the following:

$$C_{R_iR_j}(f) = \frac{|P_{R_iR_j}(f)|^2}{P_{R_iR_i}(f)\, P_{R_jR_j}(f)}, \quad \textbf{[S6]}$$

where $P_{R_iR_j}(f)$ is the cross-spectrum between $R_i(t)$ and $R_j(t)$, and $P_{R_iR_i}(f)$ and $P_{R_jR_j}(f)$ are the power spectra of $R_i(t)$ and $R_j(t)$, respectively, and $|\ldots|$ denotes the absolute value. Then, the correlation coefficient between the two spike trains was determined as the square root of the coherence value at frequency zero as done previously (27). All spectral quantities (i.e., power spectra, cross-spectra) were estimated using multitaper techniques with six Slepian functions (28).

Similar results were obtained when instead computing the correlation coefficient between spike counts using a binwidth of 40 ms as done in other studies (26).

Nonlinear transformations of single-neuron activity. We computed nonlinear transformations of the single-neuron activity as quantified by the response $R(t)$. These consisted of half-wave rectification, full-wave rectification, taking the Hilbert transform, and computing the variance of the neural response minus its mean value. We used the same range of sliding time windows as for computing the correlation coefficient as described above to allow for direct comparison. We considered two alternate decoders: the first linearly sums the activities of a neural population before applying a nonlinear transformation, whereas the second instead applies a nonlinear transformation to each individual neuron's response before linear summation. It is important to note that only the former decoder actually takes into account joint statistics. For example, consider N neurons with responses [R_i]. The first decoder's output, assuming that the nonlinear transformation is taking the variance, is then the following:

$$\begin{aligned} VAR\left(\sum_{i=1}^{N} R_i\right) &= \sum_{i=1}^{N}\sum_{j=1}^{N} COV(R_i, R_j) \\ &= \sum_{i=1}^{N} VAR(R_i) + 2\sum_{i=2}^{N}\sum_{j=1}^{i-1} COV(R_i, R_j), \end{aligned} \quad \textbf{[S7]}$$

where $COV(\ldots)$ is the covariance [note that $COV(X,X) = VAR(X)$ by definition]. In contrast, the output of the second decoder is as follows:

$$\sum_{i=1}^{N} VAR(R_i). \quad \textbf{[S8]}$$

Comparing Eqs. **S7** and **S8** reveals that the only difference between the outputs of both decoders is that the first one explicitly takes into account any covariation between the neural activities (i.e., "cross-terms"), whereas the second one does not.

We also computed the cross-correlation function between the response $R(t)$ and the envelope $E(t)$. This cross-correlation was normalized to have a value of 1 when cross-correlating a given signal with itself. To assess whether the cross-correlation obtained from the spiking activity of a given neuron was significantly different from zero, we generated 1,000 surrogate spike trains with the same statistics as that obtained from the neuron in question that were, by construction, uncorrelated with the envelope signal. These were obtained by obtaining the sequence of interspike intervals from the spike times, randomly permuting these, and then generating a sequence of surrogate spike times as done previously (10). The 95% confidence interval was obtained from the Gaussian probability distribution of the cross-correlation functions obtained from the surrogate spike trains. We found that, for all neurons in our dataset, the cross-correlation function was within the confidence interval. Significance was assessed using a Kolmogorov–Smirnov test.

Variance-accounted-for. We used the variance-accounted-for (VAF) to quantify whether there was a significant relationship between the envelope $E(t)$ and either of the correlation coefficient CC (VAF_{CC}), the firing rate FR (VAF_{FR}), or nonlinear transformations

of the single-neuron activity or time-dependent firing rate (VAF_{NL}). For electrosensory afferents, the VAF was averaged over pairs of afferents that were simultaneously recorded from as well as over all possible combinations of paired nonsimultaneous recordings (Fig. 1), and over pairs for which the CVs as well as the baseline firing rates of both neurons did not differ more than 0.2 (CV), and 143 Hz (baseline firing rate) from one another (Fig. 4). Because we did not record simultaneously from pairs of vestibular afferents, we averaged the VAF over all possible combinations of paired nonsimultaneous recordings in Fig. 3 of the main text. To test the effects of variability on envelope coding, we averaged the VAF over pairs for which the CV values of each afferent differed by less than 0.1 in Fig. 4 of the main text. We note that considering only these pairs did not give rise to significant differences in the performance of correlated activity at coding the envelope for both electrosensory ($P = 0.28$, rank sum test, df = 161) and vestibular afferents ($P = 0.75$, rank sum test, df = 164).

Specifically, the VAF was computed as follows:

$$VAF = 1 - \left(\frac{\mathrm{var}(y_i - \hat{y}_i)}{\mathrm{var}(y_i)} \right), \qquad \textbf{[S9]}$$

where var is the variance, $[y_i]$ is the data, and $[\hat{y}_i]$ is the predicted data. To get the predicted data $[\hat{y}_i]$, we did a linear fit of either the correlated activity $|\rho(T_k)|$ of the two neurons to the mean stimulus envelope $[E_{mean}(T_k)]$ for VAF_{CC}, or of the firing rate $[FR(T)]$ to the mean stimulus envelope $[E_{mean}(T_k)]$ for VAF_{FR}. The firing rate was computed using the same sliding window procedure as for the correlation coefficient. We systematically varied the sliding time window between 5 ms and 15 s, and computed the VAF between the correlation coefficient and the stimulus $S(t)$ as well as that between the firing rate and the stimulus $S(t)$.

To test whether VAF values obtained for driven activity (i.e., neuronal activity in response to the stimulus) were significant, we compared them to VAF values obtained for resting neuronal activity (i.e., neuronal activity when no stimulus is present). Specifically, because VAF values cannot be negative when estimated from the best linear model, a small positive bias was obtained for resting neuronal activity. This bias was then subtracted from VAF values obtained using driven activity.

Resting discharge variability. We computed spike train variability by using the coefficient of variation (CV) during baseline activity (i.e., with no stimulus present) of the neurons as follows:

$$CV = \frac{std(ISI_i)}{mean(ISI_i)}, \qquad \textbf{[S10]}$$

where std is the SD, and ISI_i the interspike interval during baseline activity before the stimulus onset. Because neurons in a given pair displayed different coefficients of variation, we estimated the variability of each pair as follows:

$$\overline{CV} = \sqrt{CV_{N1} \times CV_{N2}}, \qquad \textbf{[S11]}$$

where CV_{N1} and CV_{N2} are the CVs of the baseline activity from each neuron of a pair.

Resting discharge rate. The resting discharge rate was assessed for each afferent. We found no significant correlations between resting discharge rate and CV for both electrosensory ($R = -0.25$, $P > 0.01$, $n = 32$) or vestibular ($R = -0.09$, $P > 0.01$, $n = 18$) afferents.

For statistical purposes, the data were collected from more than one animal for each species (two monkeys and five weakly electric fish). The neuronal sample sizes were 16 pairs for electrosensory and 44 pairs for vestibular afferents, if not stated otherwise. Unless otherwise stated, the statistical significance ($P < 0.05$) was determined using nonparametric analysis with two-tailed Wilcoxon test. Before statistical analysis, the normality of the distributions was evaluated by using a Kolmogorov–Smirnov test. Data are expressed as mean ± SEM.

Modeling. We built a model consisting of two linear leaky integrate-and-fire neurons (29) receiving a common stimulus and independent noise sources. We used spiking neuron models rather than models of the time-dependent firing rate [e.g., linear–nonlinear cascade models (30)] as our experimental results show that the spiking activities are more similar when the envelope is high than when it is low. Both model neurons were described by the following equations:

$$\begin{aligned} C_1 \frac{dV_1}{dt} &= -g_1 V_1 + I_{bias,1} + S(t) + \xi_1(t) \\ C_2 \frac{dV_2}{dt} &= -g_2 V_2 + I_{bias,2} + S(t) + \xi_1(t) \\ V_1(t) \geq \theta_1 &\rightarrow V_1(t^+) = 0 \\ V_2(t) \geq \theta_2 &\rightarrow V_2(t^+) = 0, \end{aligned} \qquad \textbf{[S12]}$$

where V_1 and V_2 are the membrane voltages of neurons 1 and 2, respectively. g_1 and g_2 are the membrane conductances, C_1 and C_2 are the membrane conductances. $I_{bias,1}$ and $I_{bias,2}$ are bias currents, $S(t)$ is the stimulus, and $\xi_1(t)$ and $\xi_2(t)$ are Gaussian white-noise processes with zero mean and SDs σ_1 and σ_2, respectively, that are uncorrelated with each other and with the stimulus $S(t)$. When $V_j(t)$ is greater or equal than the threshold θ_j ($j = 1, 2$), V_j is immediately reset to 0 mV, maintained there for the duration of the absolute refractory period $T_{R,j}$, and a spike is said to have occurred at time t. As in the experimental data, the stimulus $S(t)$ consisted of 0–20 Hz low-pass–filtered (eighth-order Butterworth) Gaussian white noise with zero mean and SD σ_{stim} that was modulated by a second low-pass–filtered (0.05 Hz cutoff frequency) white noise with mean 1 and SD 0.9. The model was simulated using an Euler–Maruyama integration algorithm (31) with time step $dt = 0.025$ ms. Parameter values used, unless otherwise specified, were as follows: $g_1 = g_2 = 0.5$ mS/cm^2; $C_1 = C_2 = 1$ μF/cm^2; $I_{bias,1} = I_{bias,2} = 10$ μA/cm^2; $\theta_1 = \theta_2 = 11$ mV; $T_{R,1} = T_{R,2} = 2$ ms; $\sigma_1 = \sigma_2 = \sigma_{noise} = 2.4$ μA/cm^2, $\sigma_{stim} = 1.5$ μA/cm^2. The noises $\xi_1(t)$ and $\xi_2(t)$ were independent and thus uncorrelated. The spiking responses from the model neurons were analyzed in the same way as the experimental data.

For the simulations described in Fig. 4 of the main text, we covaried the bias currents $I_{bias,1} = I_{bias,2}$ and the noise intensities $\sigma_1 = \sigma_2$ to make the baseline firing rate approximately independent of resting discharge variability, as was observed empirically in both electrosensory and vestibular datasets. Specifically, $I_{bias,1} = I_{bias,2}$ and $\sigma_1 = \sigma_2 = \sigma_{noise}$ were set to (in microamperes per square centimeter) [1 1.24 1.55 1.92 2.39 2.97 3.70 4.60 5.71 7.10 8.83 10.98 13.66 16.98 21.11 26.25 32.64 40.59 50.47 62.75 78.02 97.02 120.64 150] and [1.67 1.61 1.54 1.48 1.41 1.34 1.28 1.21 1.15 1.08 1.02 0.95 0.88 0.82 0.75 0.68 0.62 0.55 0.49 0.42 0.36 0.29 0.22 0.16], respectively.

Model Simulations. We have systematically varied model parameters to compute VAF values from the correlation coefficient and firing rate (VAF_{CC} and VAF_{FR}, respectively). Figs. S1 and S2 show the results from these simulations. We first covaried both the bias currents $I_{bias,1} = I_{bias,2} = I_{bias}$ as well as the noise intensities $\sigma_1 = \sigma_2 = \sigma_{noise}$. Fig. S1*A* shows the values of VAF_{CC} (*Left*), VAF_{FR} (*Center*), as well as the difference between the two (*Right*). It was seen that low values of the bias current and noise intensity gave rise to low and high values of VAF_{CC} and VAF_{FR}, respectively ("a" in Fig. S1*A*). To investigate the underlying reasons, we computed the firing-rate probability density as a

function of the stimulus $S(t)$ for the same parameter ranges (Fig. S1*B*, *Left*). Our results revealed that our model neurons displayed large amounts of rectification or cutoff (i.e., the probability of obtaining a firing rate equal to zero was nonzero for a large range of stimulus values; Fig. S1*B*, *Left*, white arrow), which resulted in a nonlinear relationship between the stimulus and the mean firing rate (Fig. S1*B*, white curve in *Left*). In contrast, intermediate values of the bias current and noise intensity gave rise to large values for VAF_{CC} and low values of VAF_{FR}, respectively ("b" in Fig. S1*A*). Plotting the firing-rate density (Fig. S1*B*, *Center*) showed no cutoff and the mean firing rate was a linear function of the stimulus (Fig. S1*B*, white curve in *Center*). Finally, we found that intermediate values of noise intensity and low values of the bias current gave rise to high values of VAF_{CC} and VAF_{FR} ("c" in Fig. S1*A*). Plotting the firing-rate probability density for these parameter values (Fig. S1*B*, *Right*) revealed a significant amount of cutoff (Fig. S1*B*, *Right*, white arrow), which led to a nonlinear relationship between the stimulus and the mean firing rate (Fig. S1*B*, *Right*, white curve).

We next covaried both the stimulus intensity σ_{stim} as well as the noise intensity σ_{noise}. Fig. S2*A* shows the values of VAF_{CC} (*Left*) and VAF_{FR} (*Center*), as well as the difference between the two (*Right*). We found that high values of the stimulus intensity and low values of the noise intensity led to high values for both VAF_{CC} and VAF_{FR} ("a" in Fig. S2*A*). This was because such parameter regimes tended to elicit significant rectification as seen by plotting the firing-rate density (Fig. S2*B*, *Left*, white arrow), which led to a nonlinear relationship between the stimulus and mean firing rate (Fig. S2*B*, *Left*, white curve). In contrast, intermediate values of stimulus and noise intensity gave rise to high values of VAF_{CC} and low values of VAF_{FR} ("b" in Fig. S2*A*); this was again because the stimulus–firing-rate relationship was approximately linear (Fig. S2*B*, *Center*, white curve). Finally, high values of noise intensity and low values of stimulus intensity gave rise to low values of VAF_{CC} and VAF_{FR} ("c" in Fig. S2*A*). This is because the firing rate is then approximately independent of the stimulus in such regimes (Fig. S2*B*, *Right*, white curve).

In summary, we were able to find regions of parameter space for which VAF_{CC} was much larger than VAF_{FR}. In general, these corresponded to parameter regimes for which the stimulus–firing-rate relationship was approximately linear with a positive slope, which tended to occur for large values of the bias current, intermediate values of the noise intensity, and for small-to-intermediate values of the stimulus intensity σ_{stim} (Figs. S1 and S2).

1. Hitschfeld ÉM, Stamper SA, Vonderschen K, Fortune ES, Chacron MJ (2009) Effects of restraint and immobilization on electrosensory behaviors of weakly electric fish. *ILAR J* 50(4):361–372.
2. Bastian J (1996) Plasticity in an electrosensory system. I. General features of a dynamic sensory filter. *J Neurophysiol* 76(4):2483–2496.
3. Bastian J (1996) Plasticity in an electrosensory system. II. Postsynaptic events associated with a dynamic sensory filter. *J Neurophysiol* 76(4):2497–2507.
4. Bastian J, Chacron MJ, Maler L (2002) Receptive field organization determines pyramidal cell stimulus-encoding capability and spatial stimulus selectivity. *J Neurosci* 22(11):4577–4590.
5. Chacron MJ, Bastian J (2008) Population coding by electrosensory neurons. *J Neurophysiol* 99(4):1825–1835.
6. Krahe R, Bastian J, Chacron MJ (2008) Temporal processing across multiple topographic maps in the electrosensory system. *J Neurophysiol* 100(2):852–867.
7. Toporikova N, Chacron MJ (2009) SK channels gate information processing in vivo by regulating an intrinsic bursting mechanism seen in vitro. *J Neurophysiol* 102(4): 2273–2287.
8. McGillivray P, Vonderschen K, Fortune ES, Chacron MJ (2012) Parallel coding of first- and second-order stimulus attributes by midbrain electrosensory neurons. *J Neurosci* 32(16):5510–5524.
9. Bastian J (1981) Electrolocation. I. How the electroreceptors of *Apteronotus albifrons* code for moving objects and other electrical stimuli. *J Comp Physiol A Neuroethol Sens Neural Behav Physiol* 144:465–479.
10. Chacron MJ, Maler L, Bastian J (2005) Electroreceptor neuron dynamics shape information transmission. *Nat Neurosci* 8(5):673–678.
11. Scheich H, Bullock TH, Hamstra RH, Jr (1973) Coding properties of two classes of afferent nerve fibers: High-frequency electroreceptors in the electric fish, *Eigenmannia*. *J Neurophysiol* 36(1):39–60.
12. Dale A, Cullen KE (2013) The nucleus prepositus predominantly outputs eye movement-related information during passive and active self-motion. *J Neurophysiol* 109(7):1900–1911.
13. Jamali M, Sadeghi SG, Cullen KE (2009) Response of vestibular nerve afferents innervating utricle and saccule during passive and active translations. *J Neurophysiol* 101(1):141–149.
14. Cullen KE, Minor LB (2002) Semicircular canal afferents similarly encode active and passive head-on-body rotations: Implications for the role of vestibular efference. *J Neurosci* 22(11):RC226.
15. Lisberger SG, Pavelko TA (1986) Vestibular signals carried by pathways subserving plasticity of the vestibulo-ocular reflex in monkeys. *J Neurosci*6–(2):346–354.
16. Goldberg JM (2000) Afferent diversity and the organization of central vestibular pathways. *Exp Brain Res* 130(3):277–297.
17. Sadeghi SG, Chacron MJ, Taylor MC, Cullen KE (2007) Neural variability, detection thresholds, and information transmission in the vestibular system. *J Neurosci* 27(4):771–781.
18. Avila-Akerberg O, Krahe R, Chacron MJ (2010) Neural heterogeneities and stimulus properties affect burst coding *in vivo*. *Neuroscience* 168(1):300–313.
19. Stamper SA, Fortune ES, Chacron MJ (2013) Perception and coding of envelopes in weakly electric fishes. *J Exp Biol* 216(Pt 13):2393–2402.
20. Gussin D, Benda J, Maler L (2007) Limits of linear rate coding of dynamic stimuli by electroreceptor afferents. *J Neurophysiol* 97(4):2917–2929.
21. Sadeghi SG, Minor LB, Cullen KE (2007) Response of vestibular-nerve afferents to active and passive rotations under normal conditions and after unilateral labyrinthectomy. *J Neurophysiol* 97(2):1503–1514.
22. Middleton JW, Longtin A, Benda J, Maler L (2006) The cellular basis for parallel neural transmission of a high-frequency stimulus and its low-frequency envelope. *Proc Natl Acad Sci USA* 103(39):14596–14601.
23. Myers LJ, et al. (2003) Rectification and non-linear pre-processing of EMG signals for cortico-muscular analysis. *J Neurosci Methods* 124(2):157–165.
24. Savard M, Krahe R, Chacron MJ (2011) Neural heterogeneities influence envelope and temporal coding at the sensory periphery. *Neuroscience* 172:270–284.
25. Shadlen MN, Newsome WT (1998) The variable discharge of cortical neurons: Implications for connectivity, computation, and information coding. *J Neurosci* 18(10):3870–3896.
26. de la Rocha J, Doiron B, Shea-Brown E, Josić K, Reyes A (2007) Correlation between neural spike trains increases with firing rate. *Nature* 448(7155):802–806.
27. Shea-Brown E, Josić K, de la Rocha J, Doiron B (2008) Correlation and synchrony transfer in integrate-and-fire neurons: Basic properties and consequences for coding. *Phys Rev Lett* 100(10):108102.
28. Jarvis MR, Mitra PP (2001) Sampling properties of the spectrum and coherency of sequences of action potentials. *Neural Comput* 13(4):717–749.
29. Lapicque L (1907) Recherches quantitatives sur l'excitation électrique des nerfs traitée comme une polarisation. *J Physiol Pathol Genet* 9:620–635. French.
30. Chichilnisky EJ (2001) A simple white noise analysis of neuronal light responses. *Network* 12(2):199–213.
31. Kloeden PE, Platen E (1999) *Numerical Solutions of Stochastic Differential Equations* (Springer, Berlin).

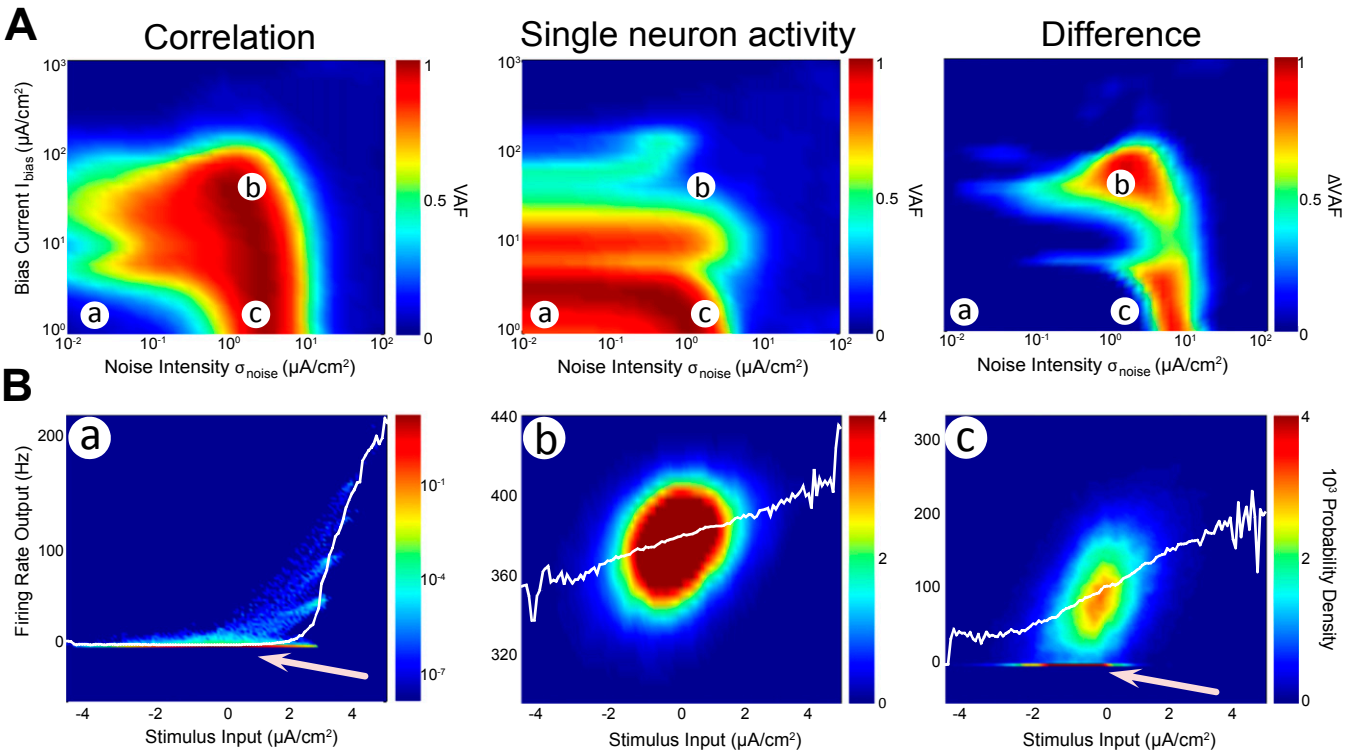

Fig. S1. Effects of bias current and noise intensity on envelope coding by correlated and single-neuron activity. (*A*) VAF values from the correlation coefficient VAF_{CC} (*Left*), from the single-neuron activity VAF_{FR} (*Center*), and the difference between the two (*Right*) as a function of the bias current and noise intensity. We focused on parameter regimes for which VAF_{CC} was low but VAF_{FR} was high (a), VAF_{CC} was high but VAF_{FR} was low (b), and for which both VAF_{CC} and VAF_{FR} were high (c). (*B*) Firing-rate probability densities (color plots) and mean firing-rate curves (white) as a function of the stimulus for the parameter regimes a, b, and c. Parameter regimes a and c both gave rise to rectification (pink arrows) and thus a nonlinear stimulus input–firing-rate output relationship. In contrast, parameter regime b gave rise to an approximately linear stimulus input–firing-rate output relationship.

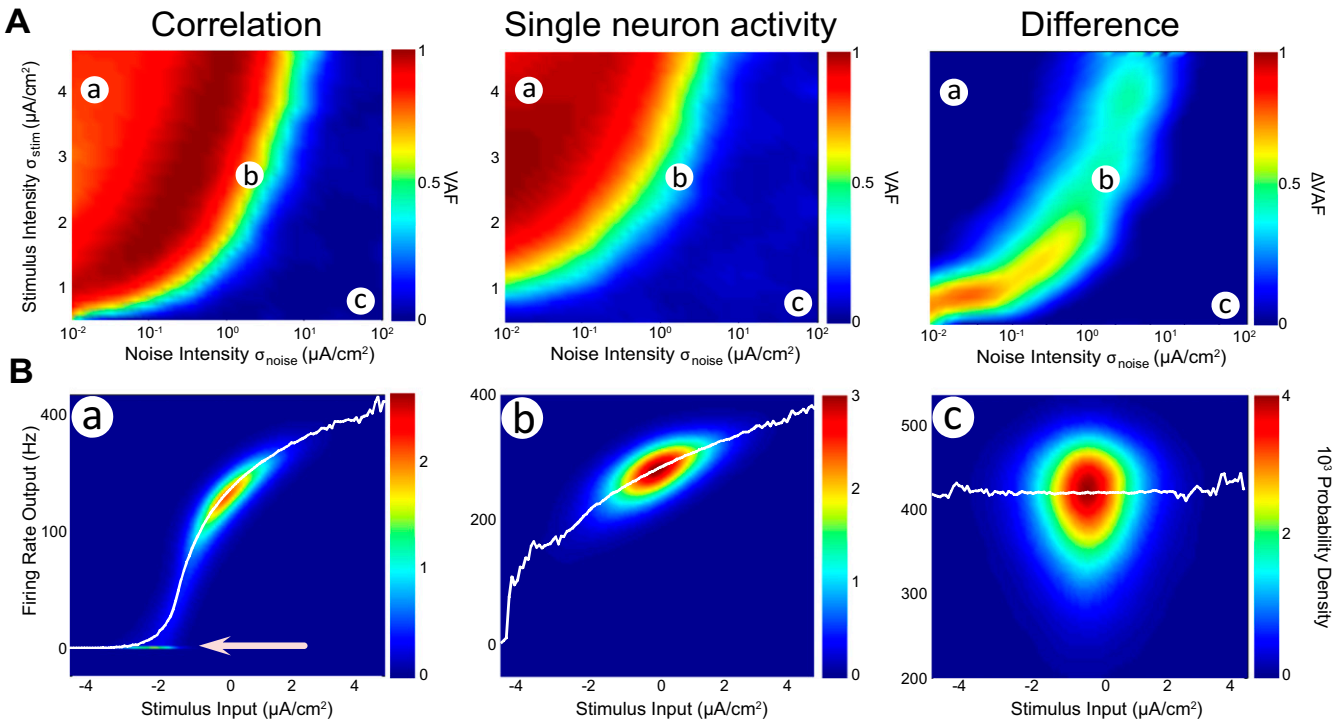

Fig. S2. Effects of stimulus and noise intensity on envelope coding by correlated and single-neuron activity. (*A*) VAF values from the correlation coefficient VAF_{CC} (*Left*) and from the single-neuron activity VAF_{FR} (*Center*), and the difference between the two (*Right*), as a function of stimulus intensity and noise intensity. We focused on parameter regimes for which both VAF_{CC} and VAF_{FR} were high (a), VAF_{CC} was high but VAF_{FR} was low (b), and for which both VAF_{CC} and VAF_{FR} were low (c). (*B*) Firing-rate probability densities (color plots) and mean firing-rate curves (white) as a function of the stimulus for the parameter regimes a, b, and c. Parameter regime a gave rise to rectification (pink arrow) and thus a nonlinear stimulus–firing-rate relationship. In contrast, parameter regime b gave rise to an approximately linear stimulus input–firing-rate output relationship. Finally, the firing rate was approximately independent of the stimulus for parameter regime c.